JOURNAL

OF THE AMERICAN CHEMICAL SOCIETY

VOLUME 106, NUMBER 13 JUNE 27, 1984

Pattern Recognition Approach to the Analysis of Geometrical Features of Solvation: Application to the Aqueous Hydration of Li^+, Na^+, K^+, F^-, and Cl^-

Francis T. Marchese*† and David L. Beveridge*

Contribution from the Department of Chemistry, Hunter College of the City University of New York, New York, New York 10021. *Received June 13, 1983*

Abstract: Statistical pattern recognition is used to analyze the results of Monte Carlo simulations for aqueous solutions of alkali metal and halide ions. The geometry of the local water structure about the lithium, sodium, potassium, fluoride, and chloride ions is determined. Lithium and sodium ions are found to be hexacoordinate with the water molecules arranged in a slightly distorted octahedron. The potassium ion is situated in a pentagonal bipyramid composed of seven water molecules. Fluoride and chloride ions are centered in a square pyramid and tricapped trigonal prism, respectively. These structures are discussed in terms of packing criteria and sensitivity of results to choice of intermolecular potentials in the simulation.

The analysis of structure in molecular liquids and fluid mixtures is complicated by the statistical nature of the problem. The system in principle is described by a statistical average of Boltzmann weighted N-particle configurations, and any rigorous definition of structure must take this into account and be defined on the statistical state of the system at a specified temperature. There is currently considerable research activity in the area of Monte Carlo and molecular dynamics computer simulations on aqueous solutions where this problem must be specifically considered in the analysis of the numerical results.[1-5]

Several recent papers from this laboratory have dealt with analyses of simulation results on molecular liquids and aqueous solutions.[6-8] A general theory for the analysis of structural and energetic indices of composition in molecular liquids has been proposed. This approach involves a partitioning of configuration space based on the Voronoi polyhedra of an isolated solute (the proximity criterion) and provides a systematic procedure for the analysis of the local solution environment of the solute molecule on the atom, functional group, or subunit basis.[7] Recently, this procedure was extended to include a description of the spatial solvent probability distributions, plotting the envelope of solvent probability density around solute atoms and functional groups. The results were referred to as "statistical state solvation sites".[8]

We describe herein a new approach to the problem, whereby elementary concepts in statistical pattern recognition are used to determine mean positions of the centers of mass of solvent molecules around a solute molecule from simulation results. The procedure is illustrated by analysis of computer simulation results on dilute aqueous solutions of monoatomic alkali metal cations Li^+, Na^+, and K^+ and the halide anions F^- and Cl^-. The results are analyzed to determine the extent to which the local hydration of the ions can be described in terms of the simple geometric arrangement of water molecules.

Background

General aspects of pattern recognition applied to chemical problems have been reviewed by Isenhour and Jurs[9] and Varzuma,[10] and interested readers are referred to these accounts for a general perspective on the field. Here, we briefly review the concepts and terminology of pattern recognition applicable to this research.

The compactness hypothesis of pattern recognition holds that objects with similar properties cluster in "feature space" and form a "class". The purpose of pattern recognition is to assign any observation to the correct class. Feature space is a d-coordinate space with axes defined by the relevent features (variables) in the experiment. In this application, the features are the (x, y, z) coordinate positions of the centers of mass of water molecules in configuration space. Thus, the Cartesian reference frame used in a liquid-state computer simulation is a 3-dimensional feature

† Present address: Department of Computer Science, Pace University, New York, NY 10038.

(1) Rossky, P.; Karplus, M. *J. Am. Chem. Soc.* **1979**, *101*, 1913.
(2) Hagler, A. T.; Osguthorpe, D. J.; Robson, B. *Science Washington, D.C.* **1980**, *208*, 599.
(3) Jorgensen, W. L.; Madura, J. *J. Am. Chem. Soc.* **1983**, *105*, 1407.
(4) Polis, G.; Corongiu, G.; Clementi, E. *Chem. Phys. Lett.* **1982**, *86*, 299.
(5) Owicki, J.; Scheraga, H. A. *J. Am. Chem. Soc.* **1977**, *99*, 7413.
(6) Beveridge, D. L.; Mezei, M.; Mehrotra, P. K.; Marchese, F. T.; Ravi-Shankar, G.; Vasu, T. R.; Swaminathan, S. In "Molecular Based Study of Fluids"; Haile, J. M., Mansoori, C. A., Eds.; American Chemical Society: Washington, DC, 1983.
(7) Mehrotra, P. K.; Beveridge, D. L. *J. Am. Chem. Soc.* **1980**, *102*, 4287.
(8) Mehrotra, P. K.; Marchese, F. T.; Beveridge, D. L. *J. Am. Chem. Soc.* **1980**, *102*, 4287.
(9) Jurs, P. C.; Isenhour, T. L. "Chemical Applications of Pattern Recognition"; Wiley-Interscience: New York, 1975.
(10) Varzuma, K. "Pattern Recognition in Chemistry"; Springer-Verlag: Berlin, 1980.

0002-7863/84/1506-3713$01.50/0

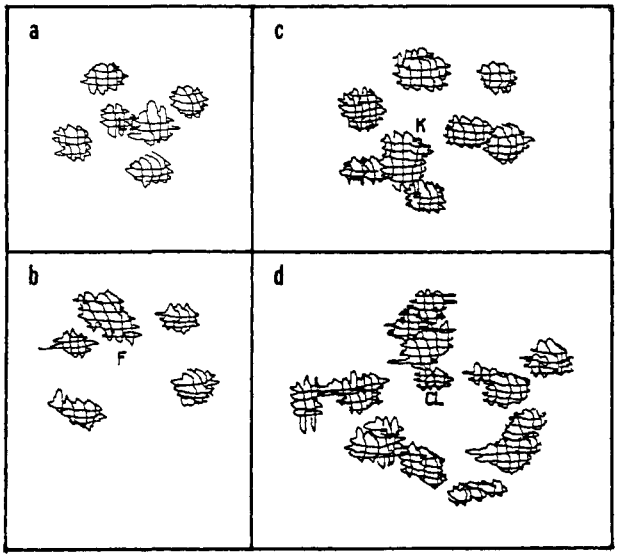

Figure 1. Statistical state solvation sites based on 90% probability densities for ion–water interactions: (a) Li^+, (b) K^+, (c) F^-, and (d) Cl^-.

space with the position of each water molecule, N, specified by a feature vector $\mathbf{R}_N$

$$\mathbf{R}_N = x_N i + y_N j + z_N k$$

the components of which correspond to three orthogonal coordinates. It now follows from the compactness hypothesis that the feature vectors in each class are in some sense nearer to all feature vectors in that class than to all or most of the vectors in the other classes and therefore occupy a "class region". When every class region is bounded and none of the class regions overlap, the classes are said to be linearly separable. The ion–water 90% 3-dimensional probability density maps (statistical state solvation sites) for the first hydration shell of Li^+, K^+, F^-, and Cl^- (Figure 1) demonstrate explicitly that linear separability between class regions holds to a very good approximation in these systems. The voids between probability clouds indicate the nonoverlap between regions in configuration space.

The clustering of feature vectors can be temporal and spatial. Temporal clustering results from the motion of a feature vector as a function of effective time about the mean position of some class region. Thus, if we were to observe the motion of a water molecule about the mean position of a solvation site during the course of a simulation we would see a temporal cluster develop. Spatial clustering follows as a consequence of temporal clustering and involves the ordering of temporal clusters in a specific volume of space. For example, the octahedral arrangement of six temporal clusters about one ion and the tetrahedral arrangement of temporal clusters about another are examples of two classes of spatial clusters.

Feature vectors are assigned to classes by means of a device or process which sorts data into categories or classes called a "classifier". The classifier assigns every feature vector to a particular decision region D_j in feature space by means of a set of decision hyperplanes. For linearly separable classes in 3-space, a plane can be placed so that it separates that region from all other class regions. If there are m classes then there are $^1/_2(m(m-1))$ possible linear boundaries. However, each assignment may not correspond to a correct or desirable classification. Thus, a classifier which attempts to minimize the number of incorrect classifications by adjusting the set of decision regions $\mathbf{D}$

$$\mathbf{D} = \{D_1, D_2, D_3, ..., D_k\}$$

is called a "trainable classifier".

Often the decision hypersurface of a classifier is determined by a set of discriminant functions $d_j(\mathbf{R}_N)$, given the following condition

$$D_j = \{\mathbf{R}_N | d_j(\mathbf{R}_N) \geq d_k(\mathbf{R}_N) \text{ for all } k\}$$

Simply stated, a feature vector $\mathbf{R}_N$ is classified into class region D_j if the value of $d_j(\mathbf{R}_N)$ is greater than $d_k(\mathbf{R}_N)$ for all other regions D_k. Between any two linearly separable classes, $d_j(\mathbf{R}_N)$ has the form

$$d_j(\mathbf{R}_N) = \mathbf{W}_j^T \cdot \mathbf{R}_N = |\mathbf{W}||\mathbf{R}_N| \cos\theta$$

where $\mathbf{W}_y^T$ denotes the transpose of the decision vector (weight vector) and θ is the angle between the two vectors. Since $\mathbf{W}$ is perpendicular to the decision plane, all patterns with positive dot products lie on the same side of the plane and all vectors with negative dot products lie on the opposite side. Thus, for a classification between any two classes we have

$$\cos\theta > 0 \text{ for } -90° < \theta < 90°$$

$$\cos\theta < 0 \text{ for } 90° < \theta < 270°$$

If all feature vectors of a class form a compact cluster in feature space, then the class can be represented by the center of mass, or mean position, of the cluster. The mean position, $\mathbf{M}_k$, is then used as a prototype (template) of that class. An unknown pattern is assigned to that class which is associated with the closest coincidence of mean positions. For distance measurements between two points in the d-dimensional hypersurface, the Euclidean distance

$$\epsilon_d = [\sum_{i=1}^{3}(\mathbf{R}_{Ni} - \mathbf{M}_{ki})^2]^{1/2}$$

is used; this is known as a minimum distance classifier where the mean position of each temporal cluster becomes a reference point. Implicit in the above is the specification of a uniquely defined coordinate system centered on the solute center of mass. For a polyatomic solute, this would be taken as the Cartesian coordinate frame coincident with the principal axis of the moment of inertia tensor. In the case of a monoatomic solute, the principal axis system is not uniquely defined and, in principle, there is no means to guarantee that succeeding configurations in the Monte Carlo chain are referred to the same "principal axis" reference system. In practice, this did not turn out to be a problem, since there is little exchange diffusion of the water molecules in the ion hydration complex in the course of a 1500K realization and the convergence in the mean energy was satisfactory. Thus, it was safe to use the laboratory frame as the basis for our analysis.

In the following section we present a simple procedure for determining these reference points and the respective decision planes for each temporal cluster.

Calculations

Monte Carlo–Metropolis statistical thermodynamic computer simulation studies on dilute aqueous solutions of monoatomic cations and anions carried out several years ago in this laboratory are used to illustrate the pattern recognition procedure and to further analyze the structure of the ion-hydration complexes. The calculations were performed on systems consisting of 1 ion and 215 water molecules at 25 °C and experimental densities. The configurational energies were calculated under the assumption of pairwise additivity by means of potential functions representative of nonempirical quantum mechanical calculations of ion–water and water–water energies as developed by Clementi and coworkers. Analysis of the realization in terms of the quasi-component distribution functions of Ben-Naim for average ion–water first shell coordination numbers gave 5.97 ± 0.02 (Li^+), 5.96 ± 0.02 (Na^+), 6.27 ± 0.25 (K^+), 4.99 ± 0.10 (F^-), and 8.36 ± 0.17 (Cl^-). Full details of the simulations are given in ref 11. The results given here, as well as other simulations, depend upon the specific choices of water–water and ion–water potentials as well as the parameters of the Monte Carlo run (step size, run length, etc.). However, this method of analysis has general validity. For an idea of the sensitivity of computer simulation results to choice of potential see ref 11. Discrepancies are small but can be significant.

(11) Mezei, M.; Beveridge, D. L. *J. Chem. Phys.* **1981**, *74*, 6902.

Table I. Fluoride Ion Feature Classes

class	class occupancy (no. of waters)	av ion-oxygen dist, Å
1	1.00	2.63 ± 0.13
2	1.00	2.59 ± 0.12
3	1.00	2.61 ± 0.12
4	1.00	2.62 ± 0.13
5	1.00	2.71 ± 0.17
6	0.04	3.22 ± 0.05
7	<0.01	3.27 ± 0.05
8	0.01	3.23 ± 0.03
9	0.01	3.25 ± 0.03
10	0.02	3.24 ± 0.04

Analysis of the Monte Carlo histories was done by employing the following pattern recognition procedure, designed to determine physical clustering of feature classes within the first hydration shell of an ion from analysis of the temporal clustering of feature vectors. The procedure is as follows.

1. The history file which contained the coordinates of all the water molecules in the simulation was sorted so that only water molecules which appear within the first solvation shell (i.e., the shell defined by the first minimum in the $g_{IO}(\mathbf{R})$) remained. The cutoffs used were 2.65, 3.00, 3.30, 3.30, and 4.10 Å for Li^+, Na^+, K^+, F^-, and Cl^-, respectively.

2. The system was assumed to be at equilibrium, and thus each water molecule should be expected to fluctuate about the mean position of its own feature class. The initial mean position of each feature class was selected by assuming it corresponded to the position of each molecule in the first configuration sampled from the simulation history. If there happened to be six water molecules within the first solvation shell, for example, there would be six classes.

3. A second configuration was then selected and classified by calculating the distance between each water within it and the original configuration. An arbitrary distance cutoff was used (e.g., 1.5 Å) in order to set up additional feature classes for water molecules found to be too far away from any previously defined class. This problem would appear if the first configuration contained only six water molecules and a later configuration contained more. As a result, the procedure automatically sets up new feature classes as they appear.

4. The center of mass of each class is next revised to represent the average position of the feature vectors assigned to each class. The analysis is continued until all configurations in the realization have been classified.

This procedure can be used in a training mode, where a small subset of the realization is used to first determine the mean position of each class which then is used to analyze the remaining configurations, or it could be used in a one-step procedure. In this application, each class turned out to be so tightly packed either procedure worked well.

Since each class is nothing more than a distribution about a mean value (the cluster center of mass), many informative statistical tests can be carried out. The results of this procedure for each system comprise the total number of classes, mean ion–water distance for each class, mean water–water distances and angles, class populations, and class–class conditional populations.

Results

The results of the statistical pattern recognition procedure applied to ion hydration are collected in this section. The results for F^-_{aq} are presented in detail to illustrate the procedure, followed by descriptions of the results for Li^+, Na^+, K^+, and Cl^-.

Table I gives the number of feature classes, the fractional occupancy of each class, and the mean position of each class for the fluoride ion. Ten classes emerge from the analysis. Classes 1–5 are occupied more than 99% of the time by water molecules, while the remaining classes are only fractionally populated. Examination of the average ion–water distance for each class indicates the first five classes are nearer to the ion than the latter five. Furthermore, the fractionally occupied sites lie near the first

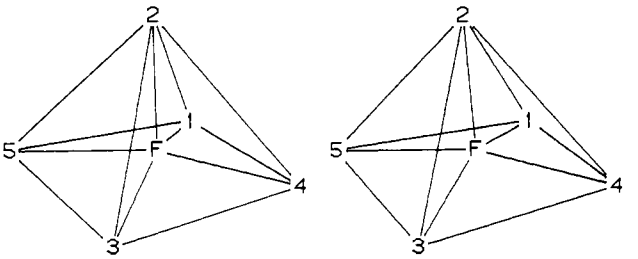

Figure 2. Stereo image of the computed mean water positions of the $F(H_2O)_5^-$ complex.

Table II. Oxygen–Oxygen Distances for $F(H_2O)_5^-$ (Å)

	2	3	4	5
1	4.13 ± 0.53	5.09 ± 0.21	3.55 ± 0.22	3.70 ± 0.23
2		4.23 ± 0.33	4.12 ± 0.22	3.98 ± 0.21
3			3.88 ± 0.18	3.62 ± 0.21
4				5.28 ± 0.22

Table III. Lithium Ion Feature Classes

class	class occupancy (no. of waters)	av ion-oxygen dist, Å
1	1.00	2.11 ± 0.15
2	0.99	2.15 ± 0.16
3	1.00	2.17 ± 0.14
4	0.99	2.14 ± 0.15
5	1.00	2.06 ± 0.10
6	1.00	2.13 ± 0.13

Table IV. Oxygen–Oxygen Distances for $Li(H_2O)_6^+$ (Å)

	2	3	4	5	6
1	2.91 ± 0.18	4.32 ± 0.20	2.98 ± 0.18	3.15 ± 0.24	3.02 ± 0.21
2		3.22 ± 0.17	4.31 ± 0.17	2.99 ± 0.16	3.03 ± 0.17
3			3.14 ± 0.20	3.02 ± 0.18	2.91 ± 0.18
4				3.09 ± 0.19	3.04 ± 0.23
5					4.22 ± 0.14

minimum in the $g_{IO}(\mathbf{R})$, the cutoff used in the analysis, and signal the region of overlap between the first and second solvation shells. Standard deviations (σ) of ion–water distances indicate little radial motion of water molecules relative to the ion.

A pictorial representation of the mean positions for the most populated classes of F^-_{aq} is shown in Figure 2. The essential feature of F^- hydration is the distorted square pyramidal structure of the $F(H_2O)_5^-$ complex. An idea of the degree of distortion can be appreciated from Table II and Figure 3. Table II contains the class–class distances and their standard deviations; Figure 3 contains the class–class angles. We see from Figure 3 that all the angles in the base of the pyramid are 90 ± 5°, confirming a square pyramidal arrangement. The σ on all class–class distances are comparable, ranging from 0.18 to 0.23 Å, with only one significant exception—the 1–2 distance has a σ of 0.53 Å. The angle defined by centers 1, F, and 3 is found to be 149° (Figure 3), midway between the value expected for a square-pyramidal (180°) and trigonal-bipyramidal (120°) arrangement. The angle defined by sites 4, F, and 5 is 160°, suggesting that the trigonal-bipyramidal structure also is populated. Note that we would expect a sixth water molecule to appear at a position beneath the base of the pyramid to form an octahedron; our results simply indicate that this molecule did not make it into the first hydration shell.

The results for the lithium cation are presented in Tables III and IV and Figures 4 and 5. Six feature classes were found at ion–water distances ranging from 2.06 to 2.17 Å. All classes are occupied essentially 100% of the time. As with the fluoride ion, Li^+–water radial motion is small, directly correlated with the strength of the ion–water potential. The stereo image of the mean water positions for the $Li(H_2O)_6^+$ system is seen in Figure 4. The

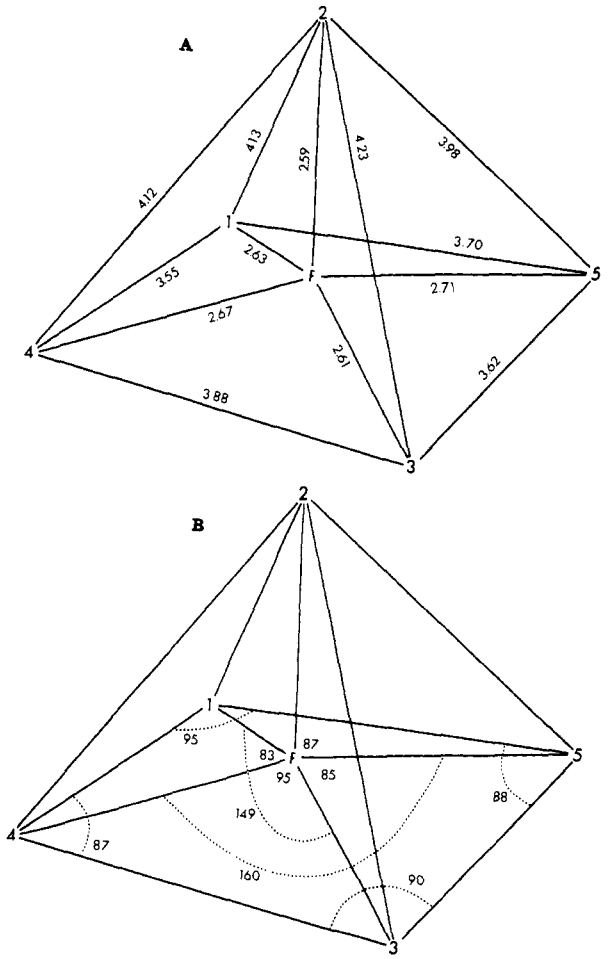

Figure 3. Average fluoride–water and water–water distances and angles in angstroms and degrees, respectively.

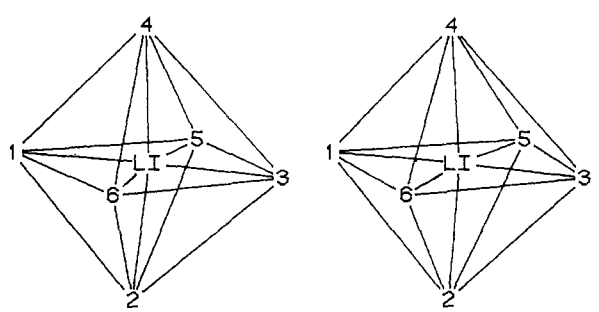

Figure 4. Stereo image of the computed mean water positions of the $Li(H_2O)_6^+$ complex.

Table V. Sodium Ion Feature Classes

class	class occupancy (no. of waters)	av ion-oxygen dist, Å
1	1.00	2.37 ± 0.13
2	1.00	2.41 ± 0.14
3	1.00	2.37 ± 0.13
4	1.00	2.35 ± 0.12
5	1.00	2.38 ± 0.12
6	1.00	2.34 ± 0.11

arrangement of water sites in the hydration complex is clearly octahedral (Figure 5). Slight distortions are seen, but the angles associated with any four apices are 90 ± 5°. Deviation in the angles between any pair of axial sites amount to about 8°. The σ values for water–water sites range from 0.17 to 0.23 Å, indicating no major fluctuations in structure.

The results for Na^+_{aq} are presented in Tables V and VI and Figures 6 and 7. As with lithium, six feature classes were found

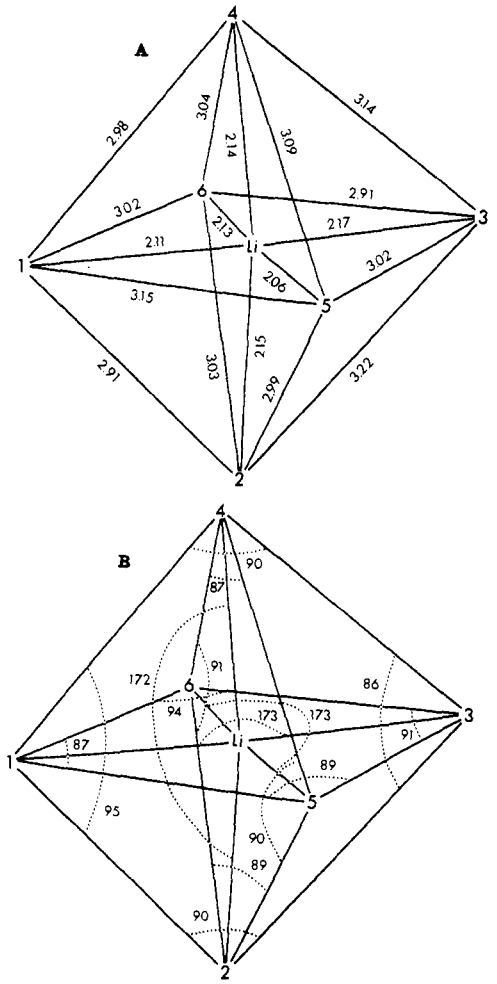

Figure 5. Average lithium–water and water–water distances and angles in angstroms and degrees, respectively.

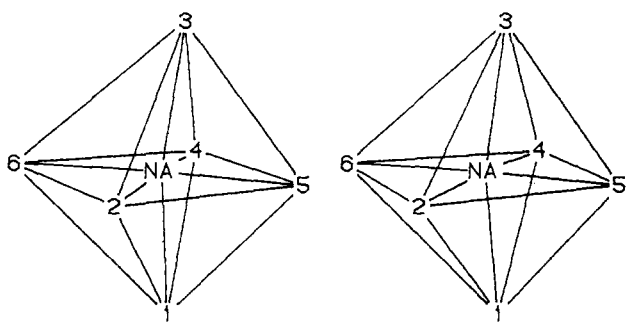

Figure 6. Stereo image of the computed mean water positions of the $Na(H_2O_6)^+$ complex.

Table VI. Oxygen–Oxygen Distances for $Na(H_2O)_6^+$ (Å)

	2	3	4	5	6
1	3.59 ± 0.25	4.75 ± 0.17	2.98 ± 0.21	3.38 ± 0.24	3.35 ± 0.23
2		3.61 ± 0.22	4.77 ± 0.18	3.28 ± 0.23	3.33 ± 0.21
3			3.37 ± 0.28	3.20 ± 0.25	3.61 ± 0.27
4				3.61 ± 0.23	3.28 ± 0.24
5					4.74 ± 0.15

at ion–water distances ranging from 2.35 to 2.41 Å. All six classes are occupied 100% of the time. The σ values for ion–water radial correlations are small (0.11–0.14 Å), again attributed to the strength of the ion–water potential. A stereo view of the mean water positions in the $Na(H_2O)_6^+$ complex is found in Figure 6. An octahedral arrangement of classes is clearly seen. Distortions in the structure are more pronounced than in the lithium complex (Figure 5), reflected in axial angle 3–Na–1 of 165°. The angles

Table VII. Potassium Ion Feature Classes

class	class occupancy (no. of waters)	av ion-oxygen dist, Å
1	0.54	3.00 ± 0.17
2	0.99	2.80 ± 0.17
3	1.00	2.74 ± 0.15
4	0.96	2.86 ± 0.16
5	1.00	2.84 ± 0.15
6	0.93	2.82 ± 0.18
7	0.89	2.97 ± 0.18
8	0.22	3.01 ± 0.15
9	<0.01	3.23 ± 0.07

defining any set of four equatorial sites deviate slightly more from 90° with a minimum of 82° and maximum of 97°. The σ for water–water distances range from 0.18 to 0.27 Å. No large fluctuations in motion are indicated.

Results for K^+_{aq} are given in Tables VII and VIII and Figures 8 and 9. Nine feature classes are found, ranging in population from <0.01 to 1.0 water molecules. Six of the classes have water molecules in residence from 89% to 100% of the time, while two have fractional occupancy. Ion–water distances range from 2.74 to 3.23 Å, the latter distances corresponding to the classes near the first-shell cutoff (populated by less than 0.01 water molecule). The σ values range from 0.15 to 0.18 Å, indicating larger radial correlations than seen in either Li^+ or Na^+. A stereoview of the $K(H_2O)_7^+$ hydration complex is in Figure 8. Here, feature classes 8 and 9 have been omitted due to low residency. The geometry appears to be a distorted pentagonal-bipyramid and looks much like an umbrella. A quantitative assessment of the structure comes from Figure 9. The apical angle (angle 2–K–5) is found to be 173°, slightly deviating from 180°. The five sites which constitute the pentagon make angles with K^+ that deviate significantly from an optimal pentagonal angle of 72°. Site occupancy suggests that $K(H_2O)_7^+$ is a greatly distorted octahedron where an additional site (occupancy 0.54) moves into the center of the edge defined by sites 4 and 6, pushing them apart and distorting the original (parent) octahedron.

Results obtained for Cl^-_{aq} are in Tables IX and X and Figures 10 and 11. Fifteen feature classes were found ranging in population from <0.01 to 1.0 water molecules. Seven classes are populated at least 98% of the time, one class 83%, and one 43%. Classes which are populated to a lesser extent will not be discussed further. The water molecules of interest are 3.2–3.88 Å from the ion. The corresponding σ range from 0.13 to 0.29 Å, slightly larger than those found for the fluoride ion. This is consistant with the decrease in the strength of the ion–water interactions in Cl^-_{aq} compared with F^-_{aq}. The stereo image for the $Cl(H_2O)_9^-$ complex is in Figure 10. The geometry corresponding to the mean positions is that of a distorted tricapped trigonal prism. The prism is defined by six water molecules forming two nearly parallel triangular faces (Figure 11), with the remaining three water molecules covering each perpendicular square face.

Finally, the site–site conditional probabilities for all five simulations showed no correlation; i.e., all sites in the first hydration shell were occupied independently and no site was occupied at the expense of another site within the shell.

Discussion

The general features of the geometry of first shell mean positions produced by the pattern recognition process are as follows. Both lithium and sodium ions are found in octahedral ligand fields.

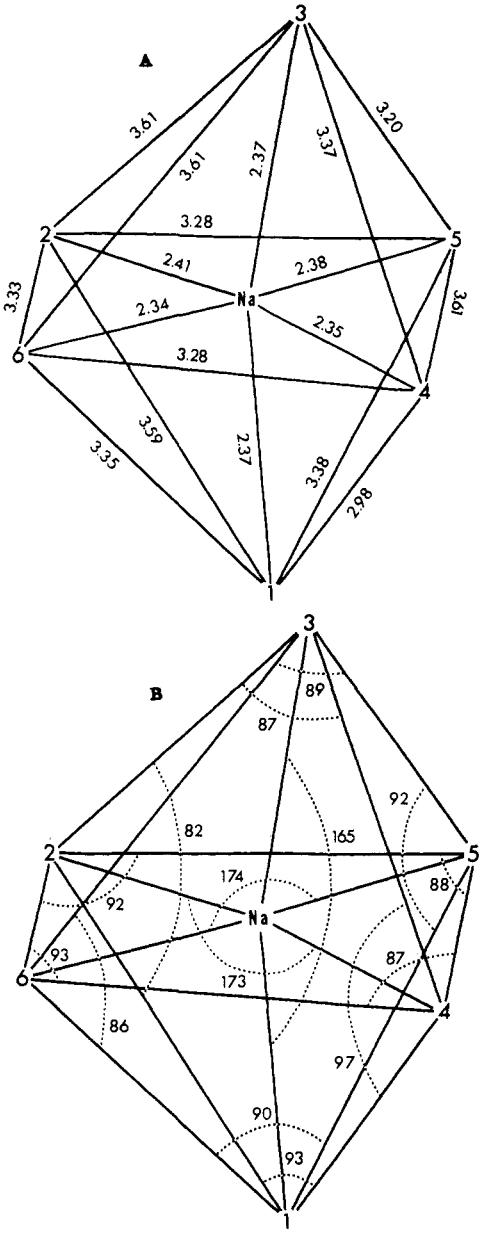

Figure 7. Average sodium–water and water–water distances and angles in angstroms and degrees, respectively.

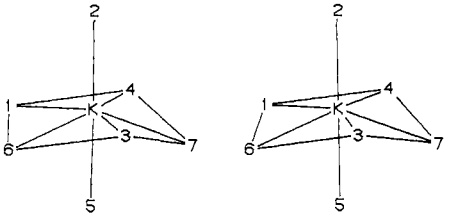

Figure 8. Stereo image of the computed mean water positions of the $K(H_2O)_7^+$ complex.

There are good correlations with the structures of crystal hydrates of these ions. For example, in $LiClO_3 \cdot 3H_2O$[12] and $NaSO_4$·

Table VIII. Oxygen–Oxygen Distances for $K(H_2O)_7^+$ (Å)

	2	3	4	5	6	7
1	4.28 ± 0.44	5.49 ± 0.26	3.61 ± 0.26	3.80 ± 0.31	2.95 ± 0.40	5.53 ± 0.23
2		4.16 ± 0.30	3.95 ± 0.40	5.65 ± 0.23	4.67 ± 0.29	4.74 ± 0.32
3			5.26 ± 0.25	4.02 ± 0.27	3.71 ± 0.27	3.44 ± 0.26
4				3.90 ± 0.20	5.29 ± 0.19	3.27 ± 0.21
5					3.41 ± 0.20	3.42 ± 0.25
6						5.40 ± 0.26

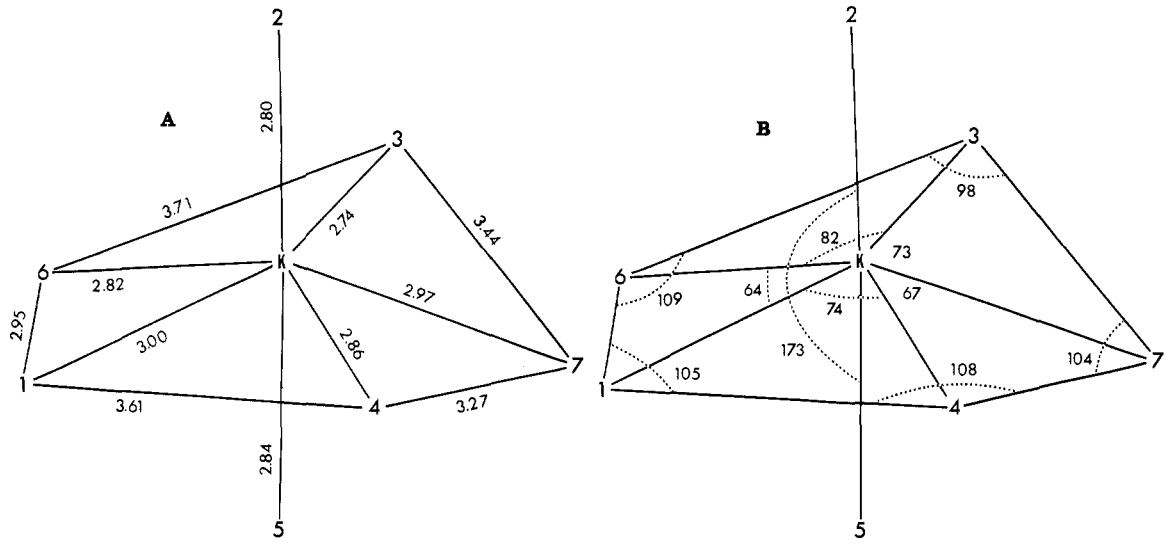

Figure 9. Average potassium–water and water–water distances and angles in angstroms and degrees, respectively.

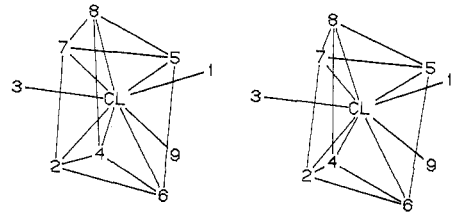

Figure 10. Stereo image of the computed mean water positions of the $Cl(H_2O)_9^-$ complex.

Table IX. Chloride Ion Feature Classes

class	class occupancy (no. of waters)	av ion–oxygen dist, Å
1	1.00	3.44 ± 0.29
2	1.00	3.20 ± 0.17
3	0.83	3.77 ± 0.20
4	1.00	3.45 ± 0.22
5	0.98	3.35 ± 0.24
6	0.98	3.53 ± 0.24
7	0.98	3.55 ± 0.24
8	1.00	3.27 ± 0.19
9	0.43	3.88 ± 0.13
10	0.28	3.98 ± 0.07
11	0.01	3.94 ± 0.05
12	<0.01	3.10 ± 0.06
13	0.19	3.86 ± 0.13
14	<0.01	3.35 ± 0.06
15	<0.01	3.97 ± 0.05

$10H_2O$[13] both Li^+ and Na^+ are octahedrally coordinated to six water molecules. The potassium ion complex does not correspond to a geometrical shape previously associated with this system. Crystal hydrates of K^+ have not been found with this geometry, yet a pentagonal-bipyramidal arrangement of oxygen donor ligands does exist in potassium hydrogen oxydiacetate.[14] The result for the chloride ion is particularly interesting, since the hexahydrated structure previously suggested for the chloride hydration complex[15] does not emerge from a pattern recognition analysis of the simulation results. This work shows that the six nearest neighbors form a prism instead of an octahedron. Three facial water molecules then complete the hydration complex. Trigonal prismatic structures such as this have been in inorganic solids and aqueous solutions of rare earth elements such as in $Nd(CH_3OH)_9^{3+}$.[16]

The pattern recognition results on mean water positions can be extended to include packing considerations, i.e., the extent to which the mean positions correspond to close packed structures. Each atomic point in space was replaced with a sphere of appropriate volume. For the water molecules, we placed a sphere which corresponds to the van der Waals radius of oxygen (1.4 Å) at the center of mass of each site. For ions, Pauling ionic radii have been used: 0.76, 0.95, 1.33, 1.36, and 1.81 Å for Li^+, Na^+, K^+, F^-, and Cl^-, respectively. The results are seen in Figures 12–16.

The lithium ion octahedron is seen in Figure 12. Figure 12a shows the entire octahedron, while Figure 12b gives the molecule with an apical water removed. There is van der Waals contact between the lithium ion and water molecules. The water molecules nearly touch; the average separation between the surfaces of the van der Waals spheres is only 0.24 Å. The sodium ion hydrate is seen in Figure 13. The octahedral structure also shows contact between the sodium ion and water molecules. The water molecules are further apart, owing to the greater size of the sodium ion. The average separation between the oxygen van der Waals spheres is 0.58 Å. The seven water molecules surrounding the potassium ion are shown in Figure 14. Because of the size of K^+ it is possible to place five water molecules in the plane around the ion. Each water essentially is in van der Waals contact with the potassium ion, as in the cases of lithium and sodium. As the size of the ion increases so does the spacing between water molecules, and for K^+, it has become possible to place a fifth water molecule in the plane around the ion.

For the anions (Figures 15 and 16), there is also contact between ion and water. The fluoride ion is more tightly bound to the five water molecules which surround it than the chloride to its nine, due to the stronger hydrogen bonds between fluoride ion and water. As with the cations, the increment in coordination number can be attributed to the size of the ion.

Two final comments should be made concerning sites and their occupancy. First, we find the time-averaged arrangement of water molecules around the ion to be nonspherical. Over a "long" time span a spherical distribution would be seen from a laboratory reference frame centered on the ion; however, structure persists when viewed, at any time, from the point of view of a local coordinate frame. Second, we have seen that many sites can have fractional occupancy, which brings up the problem of coordination

(12) Sequeira, A.; Bernal, I.; Brown, I. D.; Braggiani, R. *Acta Crystallogr., Sect. B* **1975**, *B31*, 1735.
(13) Levy, H. A.; Lisensky, G. C. *Acta Crystallogr., Sect. B.* **1978**, *B34*, 3502.
(14) Albertsson, J.; Grenthe, I. *Acta Crystallogr., Sect. B* **1973**, *B29*, 2751.
(15) Palinkas, G.; Radnai, T.; Dietz, W.; Szasz, Gy. I.; Heinzinger, K. *Z. Naturforsch. A* **1982**, *37A*, 1049.
(16) Kevan, L. *J. Phys. Chem.* **1981**, *85*, 1628.

Table X. Oxygen-Oxygen Distances for $Cl(H_2O)_9^-$ (Å)

	2	3	4	5	6	7	8	9
1	6.48 ± 0.27	6.45 ± 0.33	4.97 ± 0.43	3.83 ± 0.29	4.65 ± 0.44	6.25 ± 0.36	4.40 ± 0.33	5.02 ± 0.28
2		4.23 ± 0.34	4.40 ± 0.32	5.50 ± 0.40	3.86 ± 0.38	4.25 ± 0.32	5.84 ± 0.25	4.43 ± 0.30
3			3.66 ± 0.40	6.84 ± 0.30	6.30 ± 0.31	4.96 ± 0.44	3.64 ± 0.33	7.38 ± 0.25
4				6.72 ± 0.29	3.92 ± 0.37	6.73 ± 0.34	5.00 ± 0.35	6.36 ± 0.31
5					5.18 ± 0.38	3.81 ± 0.52	4.90 ± 0.41	3.54 ± 0.35
6						6.47 ± 0.38	6.67 ± 0.29	3.19 ± 0.29
7							4.27 ± 0.41	5.09 ± 0.36
8								6.89 ± 0.23

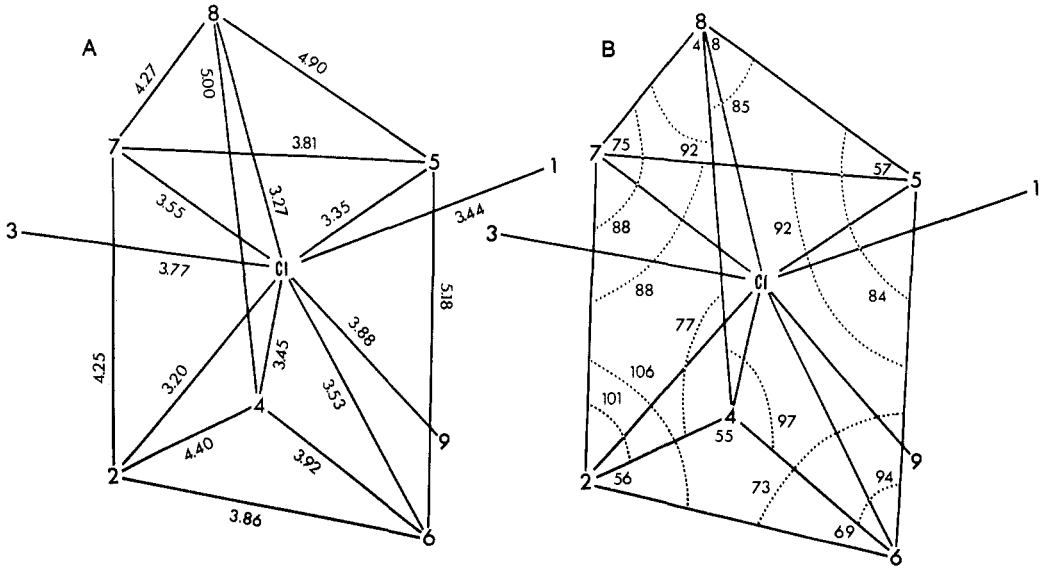

Figure 11. Average chloride–water and water–water distances and angles in angstroms and degrees, respectively.

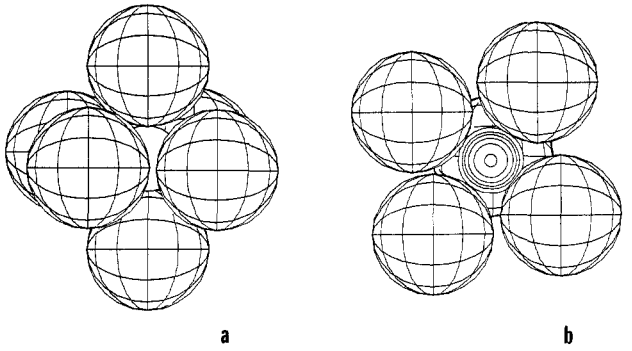

Figure 12. Space filling representation of $Li(H_2O)_6^+$ complex. Hatched spheres correspond to water molecules with van der Waals radii of 1.4 Å. (a) Complete complex; (b) complex with apical water removed.

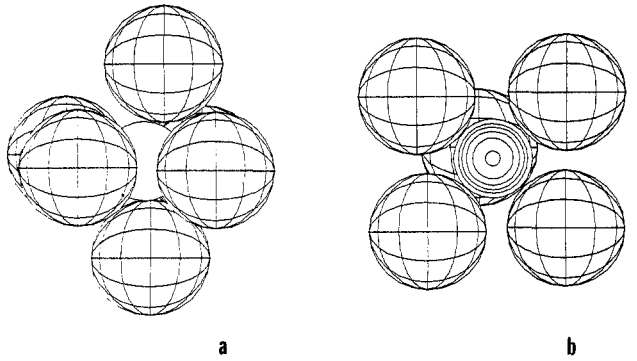

Figure 13. Space filling representation of $Na(H_2O)_6^+$ complex. Hatched spheres correspond to water molecules with van der Waals radii of 1.4 Å. (a) Complete complex; (b) complex with apical water removed.

number. If, for example, an ion has an octahedral arrangement of coordinate sites, each site being occupied only two-thirds of the time during the course of the experiment, then a coordination number of four is obtained as opposed to six. Thus, the statistical nature of the problem must be taken into consideration in any aspect of the analysis.

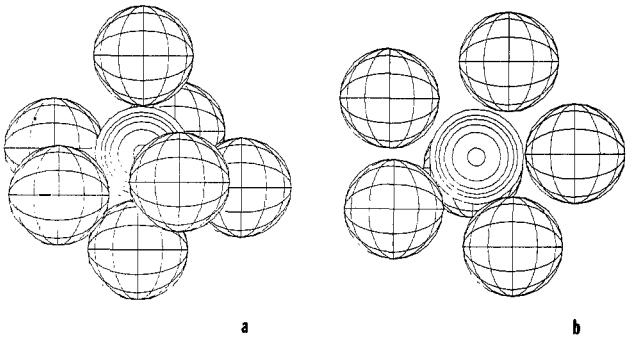

Figure 14. Space filling representation of $K(H_2O)_7^+$ complex. Hatched spheres correspond to water molecules with van der Waals radii of 1.4 Å. (b) Complex; (b) complex with apical water removed.

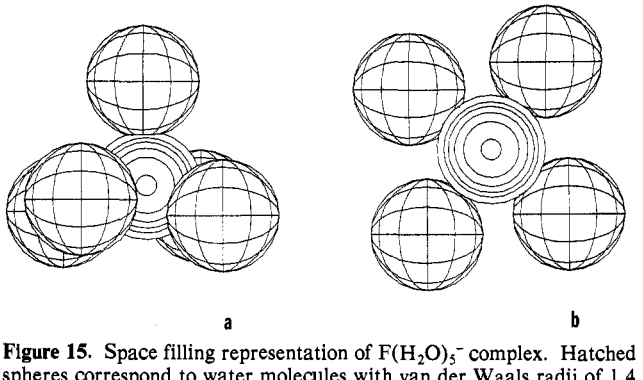

Figure 15. Space filling representation of $F(H_2O)_5^-$ complex. Hatched spheres correspond to water molecules with van der Waals radii of 1.4 Å. (a) Complete complex; (b) complex with apical water removed.

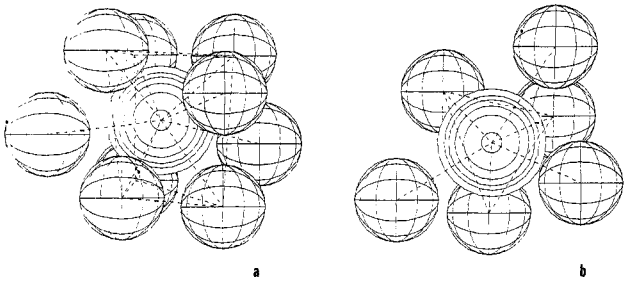

Figure 16. Space filling representation of $Cl(H_2O)_9^-$ complex. Hatched spheres correspond to water molecules with van der Waals radii of 1.4 Å. (a) Complete complex; (b) complex with top triangle removed.

Conclusions

In conclusion, we have shown that simulation results on ionic hydration can be analyzed by using elementary pattern recognition techniques and that the mean water positions in the hydration complexes can be interpreted in terms of elementary geometric polyhedra. The nature of the polyhedral structure depends significantly on the type of ion in the complex. In some cases the results are different from those expected or predicted from chemical intuition but correspond to types seen in crystal hydrate structures of various ions. Pattern recognition methods thus appear to be a useful procedure for the analysis of simulation results on fluids and provide a convenient and accessable means of considering geometrical aspects of the organization of solvent molecules in solvation shells. Most importantly, the solvent mean positions are rigorously defined on the statistical state of the fluid-phase system.

Acknowledgment. This research was supported by NIH Grant GM-12149. Computer graphics were carried out with the NIH CELS PROPHET system.

Registry No. H_2O, 7732-18-5; Li, 7439-93-2; Na, 7440-23-5; K, 7440-09-7; F^-, 16984-48-8; Cl^-, 16887-00-6.

Photochemistry of Gas-Phase $Mn_2(CO)_{10}$ and $Re_2(CO)_{10}$: Mass Spectrometric Evidence for a Dinuclear Primary Photoproduct

D. G. Leopold[†] and V. Vaida*[‡]

Contribution from the Department of Chemistry, Harvard University, Cambridge, Massachusetts 02138. *Received December 20, 1983*

Abstract: The photochemistries of $Mn_2(CO)_{10}$ and $Re_2(CO)_{10}$ following excitation at 337 nm in the region of their $\sigma^* \leftarrow \sigma$ bands are investigated under collision-free conditions. Results suggest that in addition to the $M(CO)_5$ photofragments previously reported in the molecular beam study of Freedman and Bersohn, partially decarbonylated dimetal photofragments are also produced. Thus, in the gas phase, as in solution, both dissociative CO loss and M–M bond scission appear to be primary photochemical processes in the dimetal decacarbonyl systems.

The decacarbonyldimetal complexes of manganese and rhenium were among the first metal–metal bonded systems to be subjected to a detailed photochemical investigation.[1,2] These molecules, in which the two $M(CO)_5$ subunits are joined solely by a metal–metal single bond, provide ideal systems with which to examine the competition between metal–metal and metal–ligand bond reactivity in the excited state chemistry of transition-metal carbonyl complexes. Early condensed-phase studies indicated that excitation of the allowed $\sigma^* \leftarrow \sigma$ transitions,[3] which reduce the formal metal–metal bond order from one to zero, results in clean, quantum efficent homolytic cleavage to 17-electron $M(CO)_5$ radicals.[1,2] This contrasts with the thermal decomposition pathway in the ground electronic state, which is dominated by dissociative loss of carbonyl ligands.[4]

However, recent investigations have disclosed a more complex pattern of photochemical behavior for the $M_2(CO)_{10}$ systems, involving at least two primary photoproducts whose relative yields appear to be highly sensitive to environmental effects. Flash photolysis and chemical studies suggest that CO loss[5-7] or isomerization[8] can compete with M–M bond cleavage in solution, and quantum yields as high as 30% have been estimated for the former process.[6,7] The appearance of both mononuclear and dinuclear species within 25 ps after excitation suggests that both are primary photoproducts.[5] In rigid alkane or rare gas matrices, on the other hand, only M_2-containing decarbonylated photofragments are observed upon photolysis of $Mn_2(CO)_{10}$[6] and other M–M bonded systems.[9] This has been attributed to a solvent cage effect on the efficiency of formation of solvent-separated $M(CO)_n$ species.[6,9a] In the gas phase, where such environmental perturbations are absent, dissociation of $Mn_2(CO)_{10}$ and $Re_2(CO)_{10}$ has been reported to result solely in metal–metal bond cleavage.[10]

In view of recent evidence for competing photochemical pathways in solution following one-photon near-UV excitation of dinuclear carbonyl complexes, and the results of multiphoton

[†] Present address: Joint Institute for Laboratory Astrophysics, Boulder, Colorado 80309.

[‡] Camille and Henry Dreyfus Teacher–Scholar.

(1) (a) M. S. Wrighton, J. L. Graff, J. C. Luong, C. L. Reichel, and J. L. Robbins, In "Reactivity of Metal–Metal Bonds", M. H. Chisholm, Ed., A.C.S., Washington, DC, 1981; (b) G. L. Geoffroy and M. S. Wrighton, "Organometallic Photochemistry", Academic Press, New York, 1979.
(2) M. S. Wrighton and D. S. Ginley, *J. Am. Chem. Soc.*, **97**, 2065 (1975).
(3) (a) R. A. Levenson, H. B. Gray, and G. P. Ceasar, *J. Am. Chem. Soc.*, **92**, 3653 (1970); (b) R. A. Levenson and H. B. Gray, *ibid.*, **97**, 6042 (1975).
(4) (a) H. Wawersik and F. Basolo, *Inorg. Chim. Acta*, **3**, 113 (1969); (b) J. D. Atwood, *Inorg, Chem.*, **20**, 4031 (1981); (c) N. J. Coville, A. M. Stolzenberg, and E. L. Muetterties, *J. Am. Chem. Soc.*, **105**, 2499 (1983).
(5) L. J. Rothberg, N. J. Cooper, K. S. Peters, and V. Vaida, *J. Am. Chem. Soc.*, **104**, 3536 (1982).
(6) A. F. Hepp and M. S. Wrighton, *J. Am. Chem. Soc.*, **105**, 5934 (1983).
(7) H. Yesaka, T. Kobayashi, K. Yasufuku, and S. Nagakura, *J. Am. Chem. Soc.*, **105**, 6249 (1983).
(8) (a) A. Fox and A. Poë, *J. Am. Chem. Soc.*, **102**, 2498 (1979); (b) J. L. Hughey, IV, C. P. Anderson, and T. J. Meyer, *J. Organomet. Chem.* **125**, C49 (1977).
(9) (a) R. L. Sweany and T. L. Brown, *Inorg. Chem.*, **16**, 421 (1977); (b) M. Poliakoff and J. J. Turner, *J. Chem. Soc. A*, 2403 (1971).
(10) A. Freedman and R. Bersohn, *J. Am. Chem. Soc.*, **100**, 4116 (1978).

0002-7863/84/1506-3720$01.50/0